Studies of the Ionospheric Turbulence Excited by the Fourth Gyroharmonic at HAARP

March 31 , 2015

A. Najmi[1], G. Milikh[1], Y. M. Yampolski[2], A. V. Koloskov[2], A. A. Sopin[2], A. Zalizovski[2], P. Bernhardt[3], S. Briczinski[3], C. Siefring[3], K. Chiang[4], Y. Morton[5], S. Taylor[5], A. Mahmoudian[1], W. Bristow[6], M. Ruohoniemi[7], and K. Papadopoulos[1]

[1] Departments of Physics and Astronomy, University of Maryland, College Park, MD

[2] Institute of Radio Astronomy, National Academy of Sciences of Ukraine, Kharkov, Ukraine

[3] Division of Plasma Physics, Naval Research Laboratory, Washington, DC

[4] Department of Electrical Engineering, Cornell University, Ithaca, NY.

[5] Department of Electrical and Computer Engineering, Miami University, Oxford, OH.

[6] Geophysical Institute, University of Alaska-Fairbanks, AK

[7] Department of Electrical and Computer Engineering, Virginia Polytechnic Institute, VA

Abstract. A study is presented of Artificial Ionospheric Turbulence (AIT) induced by HF heating at HAARP using frequencies close to the fourth electron gyro harmonic, in a broad range of radiated powers and using a number of different diagnostics. The diagnostics include GPS scintillations, ground based Stimulated Electromagnetic Emission (SEE), the HAARP ionosonde, Kodiak radar, and signals received at the Ukrainian Antarctic Station (UAS). The latter allowed analysis of waves scattered by the AIT into the ionospheric waveguide along Earth's terminator, 15.6 Mm from the HAARP facility. For the first time, the amplitude of two prominent SEE features, the downshifted maximum and broad upshifted maximum, were observed to saturate at ~50% of the maximum HAARP ERP. Nonlinear effects in slant total electron content (STEC), SEE, and signals received at UAS at different transmitted frequencies and intensities of the pump wave were observed. The correlations between the data from different detectors demonstrate that the scattered waves reach UAS by the waveguide along the Earth's terminator, and that they were injected into the waveguide by scattering off of artificial striations produced by AIT above HAARP, rather than via direct injection from side lobe radiation.

1. Introduction

The study of Artificial Ionospheric Turbulence (AIT) generated by high-frequency (HF) heating facilities such as EISCAT and the High-frequency Active Auroral Research Program (HAARP) has a 40-year history. Diagnostic tools to study AIT included: coherent and incoherent scattering radars to detect the formation and propagation of artificial striations, ground based electromagnetic receivers to detect Stimulated Electromagnetic Emission (SEE), scintillations of GPS signal, and detection of narrow band electromagnetic emissions via radio telescopes. At the Sura facility, Ponomarenko et al. [1999], utilized a distant broadcast station as radar while the scattered signal was received and analyzed by the UTR-2 HF Kharkov Telescope. They found that when the heating frequency exceeded a multiple of the electron gyro resonance the scattered signal underwent strong broadening (5-10 Hz), and connected it to the excitation of Super Small Striations (SSS). The experiment stimulated theoretical studies which led to the development of the SSS model [Gurevich and Zybin, 2006].

Bernhardt et al. [2009, 2011], Carozzi et al. [2002], Thide et al. [2005] and Norin et al. [2008, 2009] used SEE to probe the AIT. The broadband SEE spectra include features such as the downshifted maximum (DM) and broad upshifted maximum (BUM), both of which are indicators of the processes which occur in the ionopsheric plasma during HF heating [Leyser et al. 1989, 1993, 1994; Huang and Kuo 1994]. The DM is thought to be a signature of the parametric decay of a mode converted upper hybrid wave into another upper hybrid wave and a lower hybrid wave, while the BUM is thought to be produced by a four-wave interaction that includes upper and lower hybrid, as well as electron Bernstein modes. Recently,

Bernhardt et al [2009] and Mahmoudian et al. [2014] have used the narrow band SEE to estimate the bulk electron temperature while Najmi et al. [2014] correlated SEE measurements with analysis of GPS signals and found that the excitation of SSS coincided with the highest amplitude BUM. Additionally, Zalizovski et al [2009] performed O-mode heating at the EISCAT heater and were able to detect HF signals at the Ukrainian Antarctic Station (UAS) located 16.3 Mm away.

This paper reports the results of experiments conducted during the HAARP June 2014 campaign, whose objective was to study the development of artificial ionospheric turbulence. The data collected from the different diagnostic tools were analyzed, and the main features detected in the experiments are discussed and explained. The paper is organized as follows: In section 2, we give an overview of the experiments including the location, timing, and heating patterns. In section 3, we present experimental observations and diagnostics including measurements of phase-derived Slant Total Electron Content (STEC) using the L1/L2 GPS signals received at HAARP; measurements of SEE conducted 15 km away from the HAARP site; ionograms from the HAARP digisonde, reflectance data from the Kodiak radar and detection of the HAARP HF radiation scattered into the ionospheric channel and propagated to the receiver at the UAS in the Antarctic Peninsula. In section 4, we present a discussion of the integrated experimental results relating to the nonlinear mechanisms of pumping AIT. Finally, in section 5 we present our concluding remarks.

2. Description of Experiments

We report below observations from two daytime experiments conducted in June 6 & 7 2014, during the recent HAARP BRIOCHE campaign. The HAARP heater operated in the 0.9-

3.6 MW, power range and used O-mode polarization. The HF frequency was selected near the 4th gyroharmonic, was stepped up from 5.67 to 5.94 MHz in 30 kHz increments. (The frequency choice was dictated by the authorized frequency band allowed for the experiments). The HAARP antenna array consists of 360 crossed dipoles each fed by a 10 kW transmitter producing a total effective radiated power (ERP) of approximately 2.5 GW. Figure 1 is a schematic of the experiment, with two of ten heating cycles shown. The heating at each frequency lasted 100 s, with 20 s interpulse period, during which time an ionogram was made. Heating consisted of 10 power steps of 10 s each. The power per transmitter at each of the steps was: 2.50, 3.33, 4.17, 5.0, 5.83, 6.67, 7.5, 8.33, 9.17 and 10.0 kW, with 20 s off. In addition after the 2nd, 5th, and 7th heating cycle the heating beam direction was adjusted to track the path of the moving PRN25 GPS satellite.

The HF beam was directed toward the USA-213 GPS satellite broadcasting the PRN 25 signal, which is in a nearly circular geocentric orbit with inclination 55.0° to the equator, and radius 20.46 Mm. During the experiment, PRN 25 flew over the HAARP site daily, and the signals at both the L1 ($f_1 = 1.575$ GHz) and L2 ($f_2 = 1.227$ GHz) were measured on the ground at HAARP after traversing the HF heated region at one Hz sampling rate. As discussed in detail in our earlier paper [Najmi et al., 2014] the measured differential carrier phase was used to estimate the relative STEC. To increase the observational time from 10 min per flyover as in our 2013 experiments to 20 minutes we adjusted the heating beam direction toward the moving PRN 25 every 5 minutes. The corresponding zenith and azimuthal angles are listed in Table 1. SEE signals were measured simultaneously using an HF detector operated by the Naval Research Laboratory 15 km away from the HAARP site. The data acquisition techniques have been previously described by Bernhardt et al. [2009, 2011].

A new diagnostic technique was implemented during this campaign. The HF signals radiated by HAARP were scattered into the ionospheric waveguide by the excited artificial irregularities. This waveguide is formed between the electron density peaks of the E- and F-regions, and since the channel is above the E region, it is nearly collisionless, and waves in the channel are subject to low attenuation which allows them to be channeled to very long distances. The signal trapping and channeling is described by Erukhinov et al. [1975] and is believed to be the mechanism of very long distance propagation of EISCAT heater signals observed by Zalizovski et al. [2009].At the time of the experiment, the waveguide was oriented along the Earth's terminator and passed over both the transmitting and receiving sites simultaneously. These signals were detected on the ground at the UAS (coordinates 65.25 S, 64.25 W) 15.6 Mm away from HAARP. The HF signals were recorded within a 500 Hz frequency band centered at the carrier frequency of the HAARP signal. The data acquisition system collected records of the intensity and the Doppler spectra of the signal with time resolution 1 s and 5 s. The paper introduces a successful attempt to use the effect of long distance HF propagation for diagnostic of the AIT spectra. Finally, all the experiments were diagnosed by the HAARP iononosonde, and by the Kodiak coherent radar located 670 km South West from HAARP.

3. Experimental Observations

Each of the two experiments discussed here lasted 20 minutes, starting at about 3 UT, i.e around 7 p.m. local time. During the first day (06/06/14) the ionosphere was slightly disturbed ($\delta B \sim 50$ nT); a noticeable sporadic E-layer existed ($f_0E_s \sim 4.5$ MHz); f_OF_2 was in the frequency range 5.6-5.7 MHz while the F2 peak was located at $h_mF_2 = 270$ km. Considering

the oblique propagation of the heating wave, its frequency was reflected from the F2 peak thus, for the majority of the experiment, the heating wave was strongly absorbed in the ionosphere due to anomalous absorption. An exception was the time around 3:04 UT when the ionogram revealed that f_OF_2 dropped below 5.4 MHz, thus the heating frequency exceeded the critical frequency, and the ionosphere became transparent to the HF wave. During the second day (06/07/14) the ionosphere was also quiet (δB~30 nT) with E_s layer present. However, the ionosphere was unstable, half of the ionograms show that the f_OF_2 fell to 4.05-4.5 MHz, resulting in low absorption and absence of AIT. The remaining ionograms show f_OF_2>5.7 MHz and h_mF_2=270km, and resulting in AIT excitation.

Due to regulatory frequency constraints, the minimum heating frequency was 5.67 MHz which was above the 4th gyro resonance. In our March 2013 experiment [Najmi et al., 2014] we have obtained the resonance frequency 5.76 MHz from the SEE spectrum, at which frequency, the DM disappeared. The ionogram shows that 5.76 MHz waves are reflected at 190 km. An estimate based on the dipole model of the geomagnetic field shows that in the June 2014 experiments the 4th gyro resonance occurs at 5.6 MHz,

$$4f_{ce} = 5.76MHz\left(\frac{R_E + 190km}{R_E + 250km}\right)^3$$, where 250 km is the reflection height of 5.6 MHz taken

from ionograms. Thus the lowest heating frequency 5.76 MHz is close to the BUM cutoff, about 8 kHz above the 4th gyroharmonic, i.e. at 5.68 MHz [Leyser et al., 1994].

3.1 Observations made by the GPS detector at HAARP

Data collected by the HAARP GPS detector during HF heating experiments on June 6th and 7th are presented in figures 2 and 3. Figures 2a and 2b show STEC data in Total Electron Content Units (TECU) during heating experiments with heated on-off times indicated by

solid vertical lines as a function of the elapsed time and heating frequency for June 6th (figure 2a) and June 7th (figure 2b). The heating at each frequency lasted 100 s while each 10 s the power was stepped up. Thus, figure 2 shows STEC amplitude as a function of heating power for each of the heating frequencies. The STEC amplitude immediately increases after the heater is turned on, but after several seconds, the amplitude decays. There is additional "snap-back" after the heater is turned off. The mechanism for this behavior is discussed in detail in section 4.

Figure 3 shows the scintillation index (S_4) of the L_1 and L_2 Carrier-Noise-Ratio (CNR) on June 6th (figure 3a) and June 7th (figure 3b). Heater on-off times are indicated by solid vertical lines. Although we collect CNR, we assume that in our frequency range noise does not change greatly over our S_4 intervals, and thus the CNR is proportional to the signal intensity. In figure 3 the highest values of the S_4 index were detected between 900 and 1100 s into the heating for both L_1 and L_2 corresponding to frequencies near 5.88-5.91 MHz. The extrema of the S_4 index are known to correspond to changes in the length scale of the underlying physical processes [Whitney et al 1969] The mechanism of the change in length scales is discussed in section 4.

3.2 SEE observations

Stimulated Electromagnetic Emission (SEE) signals were measured simultaneously with the STEC using an HF detector operated by the Naval Research Laboratory 15 km away from the HAARP site and shown in Figures 4-6. Figure 4 shows the power spectral density (PSD) of the SEE emission at the selected frequency 5.76 MHz. The traces are averaged over a 10 s portion of the heating period with constant ERP. The heating frequency is shown by the

highest peak in the center at $\Delta_f = 0$, the down shifted maximum (DM) is on the left side of the heating frequency at Δ_F=-10 kHz, while the broad upshifted maximum (BUM) is on the right side of the plots in the range Δ_F=+50-150 kHz. Each are indicated by arrows. The blue trace corresponds to the per-transmitter power of 2.5 kW, green to 5.0 kW, and red to 10 kW (25, 50, and 100% respectively). We see that the peak amplitude of the SEE signal is saturated at 50% power.

In figures 5 and 6, the traces are independently normalized, but typically the intensity of the DM is comparable to the BUM at frequencies close to the gyro-resonance and up to 25 dB stronger than the BUM at higher frequencies. Figure 5 shows the amplitude of the DM and BUM as a function of the pump frequency. The red and blue traces in figure 5 show the amplitude of the BUM and DM respectively, both normalized by their peak values. The BUM reaches its peak at f_h= 5.67 MHz which is close to the BUM cutoff, and reduces with f_h. The DM reaches its peak at f_h= 5.79 MHz, stays at nearly its maximum amplitude up to 5.85 MHz, and then rolls off for f_h > 5.85 MHz. The amplitude of the BUM is observed to decay by ~ 10dB/ 100kHz while the DM both initially increases by ~12 dB / 100 kHz, saturates, then decays at 12 dB / 100 kHz. Figure 6 shows the amplitude of the PSDs normalized by their peak value as a function of the heating power for frequencies 5.67 (figure 6a) and 5.79 (figure 6b) MHz. These frequencies were chosen to demonstrate the strongest values of the BUM and DM amplitude. For both the DM and the BUM, we see 90% saturation occurs by 50% of full power.

3.3 Observations made by the Kodiak radar

Figure 7 shows data measured by the Kodiak radar during the experiments on June 6th. Figure

7a shows the SNR time series of the Kodiak radar backscattered signals. Beam 9 of the radar was directed towards the heated region at frequency of about 12 MHz. The signal reflected by the AIT is centered at 700 km slant range. During the 10th cycle at 03:12:00-03:14:30, the SNR was strongly reduced because the Kodiak beam 09 was almost outside of the HF heating spot. This was a geometric effect of the angular adjustments of the beam to track PRN 25 and this final heating cycle was picked up by beam 10. The HF heating was switched on at 02:55 followed by the buildup of the reflected radar signal over 25 s. Then a strong SNR of more than 50 dB was detected.The reflection increased by ~10 dB around 02:57 then reduced around 03:00 and 03:04 due to decrease in the ionospheric plasma density. The second dip was discussed in section 3, while the first dip occurred at a time not covered by the ionograms at HAARP. Between 03:11:30 and 03:13:30 the SNR decreased, and at 03:14:30 the heater was switched off and the reflection gradually disappeared. Figure 7b shows time series of the velocity of the ionospheric irregularities. Starting at 02:55:00, the irregularities quickly accelerate to 35-40 m/s, peak at ~60 m/s near 02:57:00-02:59:00, when the heating frequency f_h=5.70 MHz was close to the value of f_OF_2 obtained from ionograms and the double resonance, where the pump frequency matches both the local upper hybrid frequency and an integer multiple of the electron cyclotron frequency, condition was fulfilled, then gradually reduces to ~30 m/s at later times. During June 7th, radar reflection was weak and is not shown.

3.4 HAARP signals detected at UAS

Monitoring of the HAARP HF signals was carried out at the UAS "Academician Vernadsky". Figure 8a and 8b show the spectrogram of the received signal for June 6th and June 7th, while figure 9 shows the signal-to-noise-ratio of the signal as a function of time detected on June 6th. The 8th (f_h = 5850 kHz) and 9th (f_h = 5910 kHz) heating cycles, indicated by black

arrows at the spectrograms, were contaminated by interference signals and therefore were not processed in figure 9.The blue trace shows the measured data while the red trace is the 10s moving average. The intensity of detected signal strongly depends on the heating frequency f_h. For f_h slightly above the 4th gyro-frequency the intensity of the detected signal was very low, barely above the noise level. The intensity of the detected signal increased with f_h and peaks at 5.79 MHz. We were unable to detect scattered HAARP HF signals from similar detectors in Ukraine and Scandinavia, thus verifying the role played by Earth's terminator in the formation of the waveguide. Figure 10 shows that for frequencies 5.67-5.73 MHz, the signal intensity is approximately linear in HAARP's ERP, where for frequencies 5.76-5.88 MHz the signal intensity is nonlinear. The blue trace in figure 10 shows the time dependent received signal intensity, the red trace shows the linear fit, and the green trace shows a reference linear fit with a four times increase in the received signal.. Similar results were obtained on June 7 except that the signal-to-noise ratio was by 5-10 dB less than that on June 6 (see figures 8a and 8b). In figure 11, we show a close-up of the received signal at two different frequencies, in blue, 5.70 MHz where the received signal is linear in HAARP's ERP, and in red, 5.79 MHz, where the received signal is non-linear. The error bars are the standard deviation of the mean of the SNR detected at UAS.

The spectral width as a function of the heating frequency is shown in figure 12 for each of 100 s time interval which correspond to the heating by a chosen frequency on June 6th. The spectral width at half power was obtained by using smoothed spectral curves, and the average spectral width is ~1.1 Hz, and in all cases is below 1.5 Hz. O. Finally, figure 13 presents the S_4 scintillation index as a function of the heating frequency over each 100 s time interval. The extrema of the S_4 index are known to indicate changes in the scales of the underlying causes of turbulence, and the first peak at f_h=5.73 MHz corresponds to when the SSS, indicated by

the BUM (see figure 5), begin to be supressed by the longer scale striations indicated by the presence of the DM which can effectively scatter the HF waves. The second peak at 5.82 MHz is isolated due to signal interference, and it is not clear if it is a local extrema, but we speculate that it is and that it corresponds to the pump frequency at which dekameter scale striations are no longer efficiently pumped.

4 Discussion

The main features detected in the experiments including theoretical considerations are discussed below.

Earlier, in figure 2, we showed the dependence of the STEC amplitude in TECU with radiated HF power for the June 6th and June 7th experiments. We expected that the STEC amplitude would increase with ERP because larger ERP can lead to production of additional SSS which modulate the GPS signal. Instead, we found that the STEC amplitude intially increased with HF power, but then at each frequency it decayed with power for power levels above ~40-50%.

A possible explanation for the nonlinear effect in the STEC amplitude is a competition between processes that form SSS, which modulate the GPS signal, and those that form decameter scale striations which control the anomalous absorption and are detected by Kodiak. A similar competition was seen by Frolov et al. [1997] when probing the region of the ionosphere heated by the Sura facility with two radars of different frequencies. The radars detected the temporal evolution of striations of size 3 and 13 m perpendicular to the geomagnetic field. It was found that the 3 m scale striations experience fast rise reaching a peak in 3 s, and then become suppressed by the rising 13 m scale striations, which gradually saturate in about 10 s.

Consider the following physical argument: as shown by Najmi et al. [2014] the STEC value is proportional to the amplitude of super small striations $(\delta n_e / n_e)_{SSS}$ which in turn is proportional to the pumping power P of the heating wave [Gurevich and Zybin, 2006].

$$STEC \propto \left(\frac{\delta n_e}{n_e} \right)_{sss} \propto P$$

In the prescence of dekameter scale striations produced by the anomalous absorption of the heating wave the pump power is reduced by:

$$P = P_0 e^{-\beta \left(\delta n_e / n_e \right)_{DM}^2}$$

where β is a coefficient and $\left(\delta n_e / n_e \right)_{DM}$ indicates the dekameter scale striations.

Furthermore Frolov et al. [1997] obtained that $(\delta n_e / n_e)_{DM}^2 \propto P$ for the striations with the scale size close to 10 m, and in our experiments the pumping power was varied in the range $P_{min} < P < P_{max}$, where P_{max} is the full heating power, we then transitively obtain the following STEC dependence upon the varying power

$$STEC \propto P / P_{max} e^{-\alpha P / P_{max}}$$

We found our STEC data fit this product of a linear and exponential function, with the STEC data from June 6th and least-square fit shown in figure 14, and the parameter α determined from the power that corresponds to the STEC peak value, At the STEC peak we have $d (STEC) / dP = 0$, thus $\alpha = (P_{peak} / P_{max})^{-1} = \left(34/100 \right)^{-1} = 2.94$.

A separate effect of interest comes from the SEE observations. In figure 15, we show the peak amplitudes of PSDs as a function of the heating frequency f_h. The BUM amplitude,

indicated in red, decays rapidly as f_h increases, while the DM amplitude, shown in blue, rises, saturates, then decays for much larger f_h.

Since the work by Huang and Kuo [1994], it is known that the growth rate of the BUM induced instability is $\gamma \propto 1/\sqrt{(f_{UH}^2 - f_{EB}^2)}$. Where f_{UH} is the upper hybrid frequency and f_{EB} is the electron Bernstein frequency which for larger wave numbers is a multiple of the electron gyro frequency. We estimate that $\gamma \propto 1/\sqrt{(f_h - 4f_{ce})}$ where $f_h > 4f_{ce}$, and since the ionospheric conditions indicate $4 f_{ce}$=5.6 MHz, as the heating frequency increases past the resonance, the growth rate of the BUM related instability is squelched. By contrast, it is known that the DM disappears at a multiple of the electron gyro resonance. The DM amplitude increases when f_h rises above $4f_{ce}$ and eventually saturates [Kotov et al., 2008]. However at higher frequencies the value f_h could exceed the f_oF_2, thus the ionosphere becomes transparent. Since the HF beam is directed at about 16° to MZ, and the beam has a conical shape some fraction of the beam could be still absorbed while the other become transparent which reduces the overall heating effect, which can explain why we see a decay of the DM amplitude with f_h rather than a sharp cutoff.

Previous work by Carozzi et al. [2002], Wagner et al. [1999] and Frolov et al. [1997] have also made SEE observations of heating with varying ERP near the fourth gyroharmonic. Our experiments operated at 10 dBW higher ERP than that available at Sura, and probed a frequency range of 270 kHz, as opposed to 60 kHz at Sura. At Sura, the SEE showed linear dependence of the amplitude of the BUM peak with varying ERP [Wagner et al. 1999] while our experiments showed a nonlinear saturation of both the BUM and DM peaks with varying ERP, this can be seen in figure 6. We estimated ~90% saturation of the DM and BUM amplitudes occurs at ~50% of HAARP's maximum ERP. We also detected the shift of the

BUM peak towards lower frequencies at higher ERP. In figure 4, the peak of the BUM is seen to shift-down by ~25 kHz as the ERP increases from 25% to 50%, and does not appear to shift further as the ERP is increased to 100%. Neither the saturation of the BUM and DM amplitudes, nor the frequency shift of the BUM peak, are well understood, and are subjects of future studies.

Finally, we discuss and analyze the physical processes underlying the scattering of the HAARP HF waves by the AIT into the ionospheric waveguide. These waves were detected and processed at at the UAS located 16.3 Mm from the heater. Previously, Zalizovski et al. [2009] detected HF signals from the EISCAT facility at the UAS.

The received HF signal had two different components, one a narrowband "mirror-reflected" and another "scattered" having a few times wider spectrum. Zalizovski et al [2009] found that although both components propagate along the ionospheric channel, the mirror-reflected signal is associated with the side lobe radiation of the transmitting HF antenna, which bypasses the modified volume, while the scattered signal was radiated through the main antenna beam and then scattered by pump-induced plasma striations. In order to establish which of the two mechanisms is dominant one needs to sweep the heating frequency around a multiple of the electron gyro resonance. While the side lobe radiation is not sensitive to small frequency variations, the spectrum of the pumped striations, and thus the signal scattering, strongly depends on f_h.

Figure 15 shows amplitudes of PSDs obtained from the SEE spectrum combined with the intensity of the HAARP signal measured at UAS taken from the Doppler spectrum on June 6th (figure 8) as a function of the heating frequency. As we discussed above, the red and blue traces in figure 15 show the amplitude of the BUM and DM respectively at maximum heater power, both normalized by their peak values. The black trace shows the intensity of the

detected HAARP signal at UAS first smoothed by moving average (red trace in figure 8) and then normalized by its peak value. All data points are time averages over measurements taken at maximum ERP at the listed frequency and are normalized independently such that the maximum of each trace maps to 0 dB. The error bars of the black trace are the standard deviation of the mean of the SNR at UAS at maximum heater power. We found that the intensity of the signal detected at UAS during the experiments on June 6th and 7th strongly depends on the heating frequency f_h. Figure 15 reveals that on June 6th when the BUM is dominant in the SEE spectrum, it suppresses the HF signal. The stronger the BUM is, the weakerthe HF signal. By contrast, when the DM dominates in the SEE spectrum, the intensity of the detected signal increases with f_h and peaks at 5.79 MHz. Thus the DM and HF peaks occur at the same frequency.

Furthermore, it is known that the BUM is associated with the pumping of 10 cmSSS while the DM is associated with the 7-30 m scale striations [Norin et al., 2008]. Since SSS inefficiently scatter the HF waves compared to the dekameter striations related to the DM, this implies that the HAARP signal detected at UAS could be due to the scattering of the HF radiation having the half wavelength of 25 m by the decameter size artificial striations into the ionospheric channel. The Kodiak radar is sensitive to striations in this range since its half wavelength is ~10m, and it detected strong scattering in slant ranges corresponding to the HAARP facility in figure 7a, and detected striation velocity of ~30 m/s in figure 7b. This is consistent with the striation velocity calculated by the Doppler broadening at UAS, Δf_D=1.15-1.40 Hz, with corresponding velocity of irregularities $v = \dfrac{c\Delta f_D}{2f_h} = 30 - 35\dfrac{m}{s}$.

The analysis shows that the origin of the signal detected at UAS is scattering of the HAARP's

HF radiation off of artificially pumped striations and into the ionospheric waveguide. In this process, mirror reflection does not appear to play an important role, as indicated by the low amplitude of received signal at 5.67 and 5.70 MHz. Since the amplitude of the signal varied nonlinearly with the HF power at 5.76, 5.79 and 5.82 MHz, the signal cannot be induced by sidelobe radiation which is known to be linear in the radiated power.

5 Conclusions

We have presented a study of the AIT induced at HAARP by sweeping frequencies near the fourth gyro harmonic. Our study included a number of diagnostics, such as: SEE, STEC and Kodiak radar, to both verify the presence of AIT and confirm nonlinear effects related to the variation of the pump intensity and frequency. Moreover, we added the novel diagnostic of received signal at the UAS 15.6Mm away.

The AIT has a broad wavelength spectrum, and within it, we studied striations of the 10cm (SSS) and dekameter scale. These striations are indicated by the BUM and DM features respectively in the SEE spectrum. The SSS were also directly studied with GPS signals. We observed a nonlinear dependence of the STEC amplitude on the power of the HF heater. At any heating frequency the STEC amplitude first increases with ERP until it reaches a peak and then decays. This effect is due to competition between anomalous absorption, which controls the formation of dekameter striations, and instabilities which form SSS.

The SEE measurements show 90% saturation of the DM and BUM amplitude at ~50% of HAARP's maximum ERP. This is the first time this saturation has been observed, since similar previous experiments at the Sura facility were limited by a maximum ERP of 25% of HAARP's. We also observed the nonlinear dependence of the BUM and DM amplitude on

the heating frequency and found that the BUM amplitude decayed by ~10 dB / 100 kHz, while the DM amplitude first increased by 12 dB / 100 kHz, saturated, then decayed at 12 dB / 100 kHz.

We found that HF waves from HAARP were scattered by the AIT into the ionospheric waveguide oriented along Earth's terminator, analogous to a whispering gallery mode that allows the long distance propagation of waves around concave surfaces, guided in this case by the curvature of the channel between the E- and F-region electron density peaks [Budden and Martin 1962, Chang 1971], and were subsequently detected at UAS. Simultaneous attempts to measure the scattered HF signal in Ukraine and Scandinavia were unsuccessful demonstrating the critical role played by the terminator. The intensity of the received signal at UAS also has a frequency dependence, with the maximum occurring at the same frequency as the DM peak in the SEE and the minimum correlating with the BUM peak in the SEE. We also found that the signal at UAS was Doppler broadened by Δf_D=1.15-1.40 Hz, which corresponds to a velocity of ionospheric irregularities of 30-35 m/s, which is consistent with our direct measurements from the Kodiak radar.

The combination of the strong frequency dependence of the received signal at UAS, the presense of ionospheric decameter scale striations shown indirectly by SEE and directly by Kodiak, all of which are consistent with scattering off of striations, leads us to conclude that the signal detected at UAS was generated by direct scattering of the HF signal into the ionospheric waveguide at the dekameter scale artificial striations pumped by AIT, and not by mirror reflection of the sidelobe radiation.

http://ftp.astro.umd.edu/pub/SPP/HAARP_Heating_Freq_Sweep_Data/

References:

Bernhardt, P.A., C.A. Selcher, R.H. Lehmberg, S. Rodriguez, J. Thomason, M. McCarrick, G. Frazer (2009), Determination of the electron temperature in the modified ionosphere over HAARP using HF pumped stimulated Brillouin scatter (SBS) emission lines, *Annales Geophysicae*, 27, 4409-4427.

Bernhardt, P.A., C.A. Selcher, S. Kowtha (2011), Electron and ion Bernstein waves excited in the ionosphere by high power EM waves at the second harmonic of the electron cyclotron frequency, *Geophys. Res. Lett.*, 38, L19107, doi:10.1029/2011GL049390.

Budden, K.G., H.G. Martin (1962), The ionosphere as a whispering gallery, *Proc. R. Soc. Lond. A.*, 265, 554-569, doi:10.1098/rspa.1962.0042

Carozzi, T.D., B. Thide, S.M. Grach, T.B. Leyser, M. Holz, G.P. Komrakov, V.L. Frolov, E.N. Sergeev (2002), Stimulated electromagnetic emissions during pump frequency sweep through fourth electron cyclotron harmonic, *J. Geophys. Res.*, 107(A9), 1253, doi:10.1029/2001JA005082.

Chang, His-Tien (1971), The waveguide mode theory of whispering-gallery propagation in the F region of the ionosphere, *Radio Science*, 6, 4, 475-482, doi:10.1029/RS006i004p00475.

Erukhinov, L.M., S.N. Matyugin, V.P. Uryadov (1975), Radio-wave propagation in an ionospheric wave channel, *Radiophys. and Quant. Elec.*, 18(9), 958-963, doi:10.1007/BF01038191.

Frolov, V., M. Erukhimov, S.A. Metelev, E.N. Sergeev (1997), Temporal behavior of artificial small-scale ionospheric irregularities: Review of experimental results, *J. Atmos. Solar-Terr. Physics*, 59, 18, 2317-2333.

Gurevich, A.V., K.P. Zybin (2006), Strong field aligned scattering of UHF radio waves in ionospheric modification, *Phys. Lett. A.*, 358, 159-165, doi:10.1016/j.physleta.2006.05.064.

Huang, J., S.P. Kuo (1994), A theoretical model for the broad upshifted maximum in the stimulated electromagnetic emission spectrum, *J. Geophys. Res.*, 99, A10, 19569-19576.

Kotov, P. V., E. N. Sergeev, S. M. Grach (2008), Spectra of stimulated electromagnetic emission of the ionosphere upon sweeping of the pump wave frequency near gyroharmonics. I. Experimental results, *Radiophys Quantum Electronic, 51,* 417-430, doi: 10.1007/s11141-008-9043-5.

Leyser, T.B., B. Thide, H. Derblom, A. Hedberg, B. Lundborg, P. Stubbe, H. Kopka (1989), Stimulated electromagnetic emission near electron cyclotron harmonics in the ionosphere, *Phys. Rev. Lett.*, 63,11.

Leyser, T.B., B. Thide, M. Waldenvik, S. Goodman, V.L. Frolov, S.M. Grach, A.N. Krashtin, G.P. Komrakov, D.S. Kotik (1993), Spectral structure of stimulated electromagnetic emissions between electron cyclotron harmonics, *J. Geophys. Res.*, 98, A10, 17595-17606.

Leyser, T.B., B. Thide, M. Waldenvik, E. Veszelei, V.L. Frolov, S.M. Grach, G.P. Komrakov (1994), Downshifted maximum features in stimulated electromagnetic emission spectra, *J. Geophys. Res.*, 99, A10, 19555-19568.

Mahmoudian, A., W.A. Scales, P.A. Bernhardt, B. Isham, E. Kendall, S.J. Briczinski, N.E.B. Fuentes, O. Vega-Cancel (2014), Electron gyro-harmonic effects on ionospheric stimulated brillouin scatter, *Geophys. Rev. Lett.*, 41, 16, 5710-5716, doi:10.1002/2014GL06105U.

Najmi, A.C., G. Milikh, J. Secan, K. Chiang, M. Psiaki, P. Bernhardt, S. Briczinski, C. Siefring, C.L. Chang, K. Papadopoulos (2014), Generation and detection of super small striations by F region HF heating, *J. Geophys. Res. Space Physics*, 119, 7, 6000-6011, doi:10.1002/2014JA020038.

Norin, L., S.M. Grach, T.B. Leyser, B. Thide, E.N. Sergeev, M. Berlin (2008), Ionospheric plasma density irregularities measured by stimulated electromagnetic emission, *J. Geophys. Res.*, 113, A09314, doi:10.1029/2008JA013338.

Norin, L., T.B. Leyser, E. Nordblad, B. Thide (2009), Unprecedentedly strong and narrow electromagnetic emissions stimulated by HF radio waves in the ionosphere, *Phys. Rev. Lett.*, 102, 065003, doi: 10.1103/PhysRevLett.102.065003.

Ponomarenko, P.V., T.B. Leyser, B. Thide (1999), New electron gyroharmonic effects in the HF scatter from pump-excited, field-aligned ionospheric irregularities, *J. Geophys. Res.*, 104A, 10081-10087, doi: 10.1029/1999JA900039.

Sergeev, E. N., V. L. Frolov, G. Komrakov, B. Thide and T. Carozzi (1997), Temporal evolution of HF-excited plasma waves, measured at different pump frequencies by stimulated electromagnetic emission (SEE), *J. Atmosph. & Solar Terr. Phys.*, **59**, 2383-2400.

Thide, B., E.N. Sergeev, S.M. Grach, T.B. Leyser, T.D. Carozzi (2005), Competition

between Langmuir and upper hybrid turbulence in an HF pumped ionosphere, *Phys. Rev. Lett.*, 95, 25, doi: 10.1103/PhysRevLett.95.255002.

Wagner, L.S., P.A. Bernhardt, J.A. Goldstein, C.A. Selcher, V.L. Frolov, E.N. Sergeev (1999), Effect of ionospheric self-conditioning and preconditioning on the broad up-shifted maximum component of stimulated electromagnetic emission, *J. Geophys. Res.* 104, 2573-2590

Whitney, H.E., J. Aarons, R.S. Allen, D.R. Seemann (1969), Estimation of the cumulative amplitude probability distribution function of ionospheric scintillations, *Radio Science*, 7, 1095-1104, 1972.

Zalizovski, A.V., S.B. Kashcheyev, Y.M. Yampolski, V.G. Galushko, V. Belyey, B. Isham, M.T. Rietveld, C. La Hoz, A. Brekke, N.F. Blagoveshchenskaya, A. Kornienko (2009), Self-scattering of a powerful HF radio wave on stimulated ionospheric turbulence, *Radio Science*, 44, RS3010, doi:10.1029/2008RS004111.
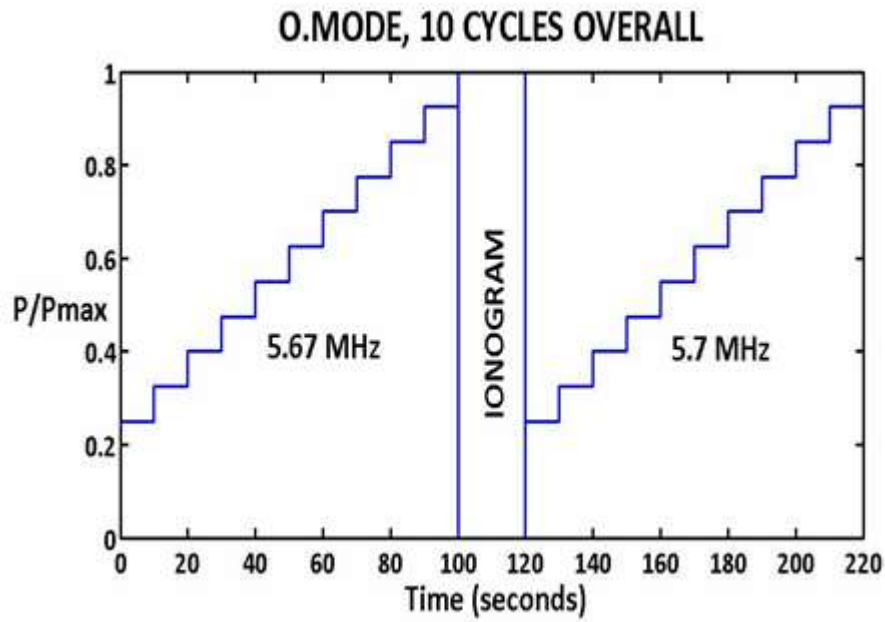
Figure 1a: Schematic of HF heating. The HAARP heater operated in the 0.9-3.6 MW, power range, used O-mode heating. The HF frequency was near the 4th gyroharmonic, and was stepped up from 5.67 to 5.94 MHz in 30 kHz increments. Here two of ten heating cycles are shown. The heating at each frequency lasted 100 s, with 20 s interpulse period, during which time an ionogram was made. Heating consisted of 10 power steps of 10 s each. The power per transmitter stepped up from 2.5 kW to 10 kW with 0.83 kW incremental.
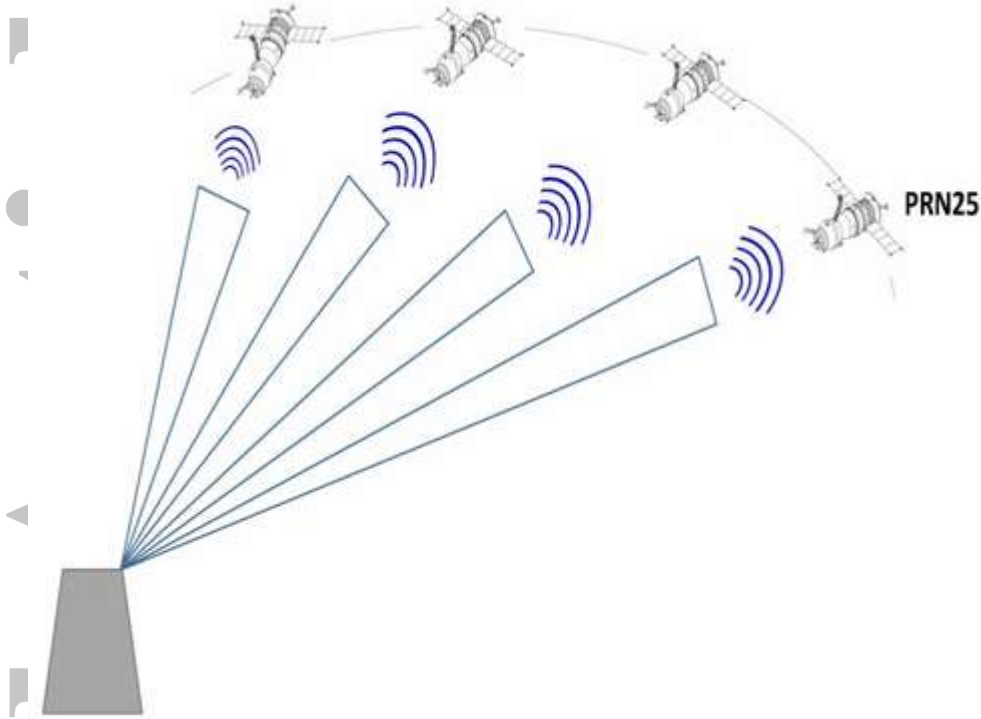
Figure 1b: The HF beam was directed toward the PRN GPS 25 satellite on a geocentric orbit. To increase the observational time we adjusted the heating beam direction toward the moving PRN 25 every 5 minutes. The corresponding zenith and azimuthal angles are listed in Table 1. .
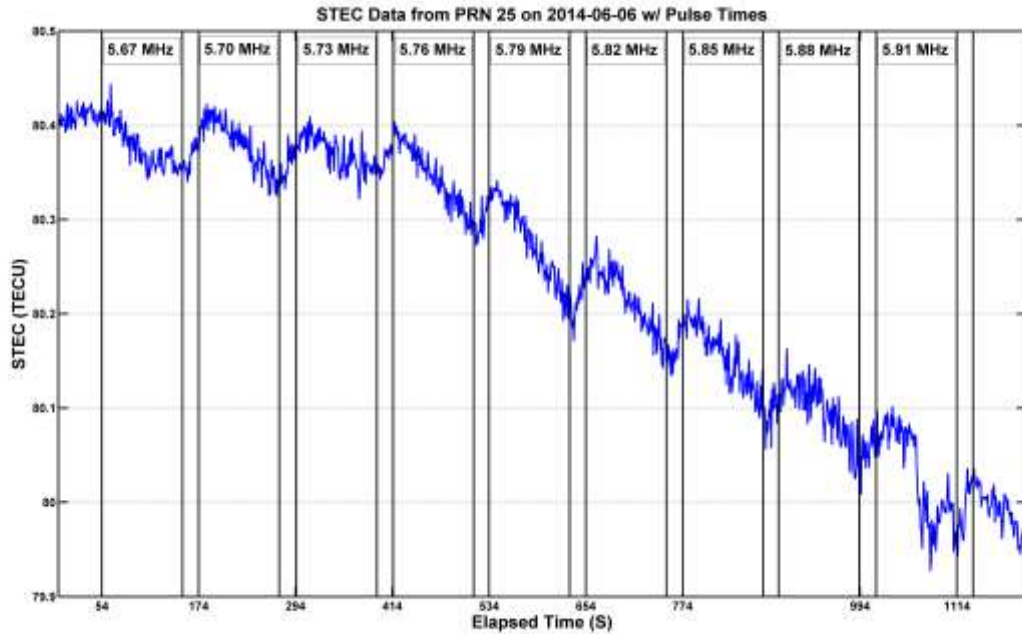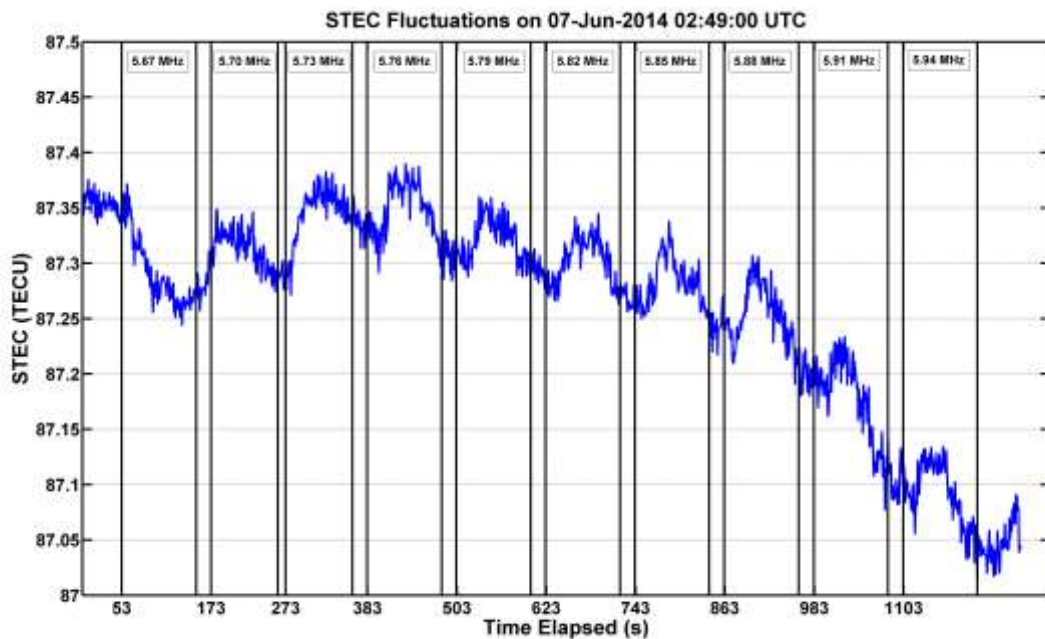
Figure 2a:

Figure 2b:

Figure 2: STEC data (in TECU) during heating experiments on June 6th (a) and June 7th (b) with heated on-off times indicated by solid vertical lines. The heater is first turned on around 20 s (a) and 50 s (b) elapsed. Since the heating at each frequency lasted 100 s and each 10 s the power was stepped up, the figure reveals STEC amplitude vs. power for each of the heating frequencies.
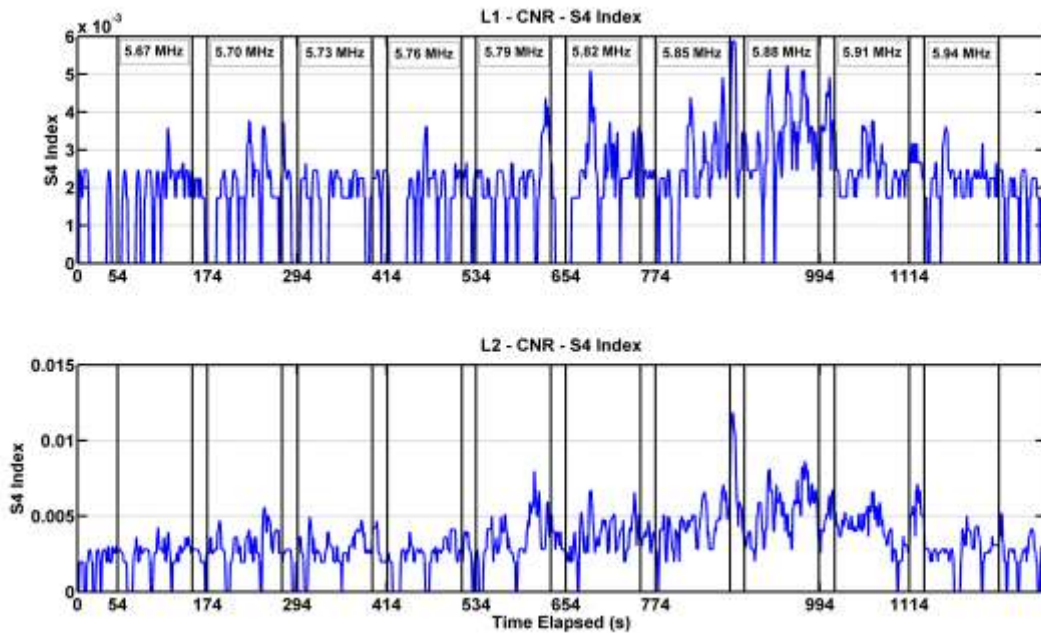
Figure 3a:
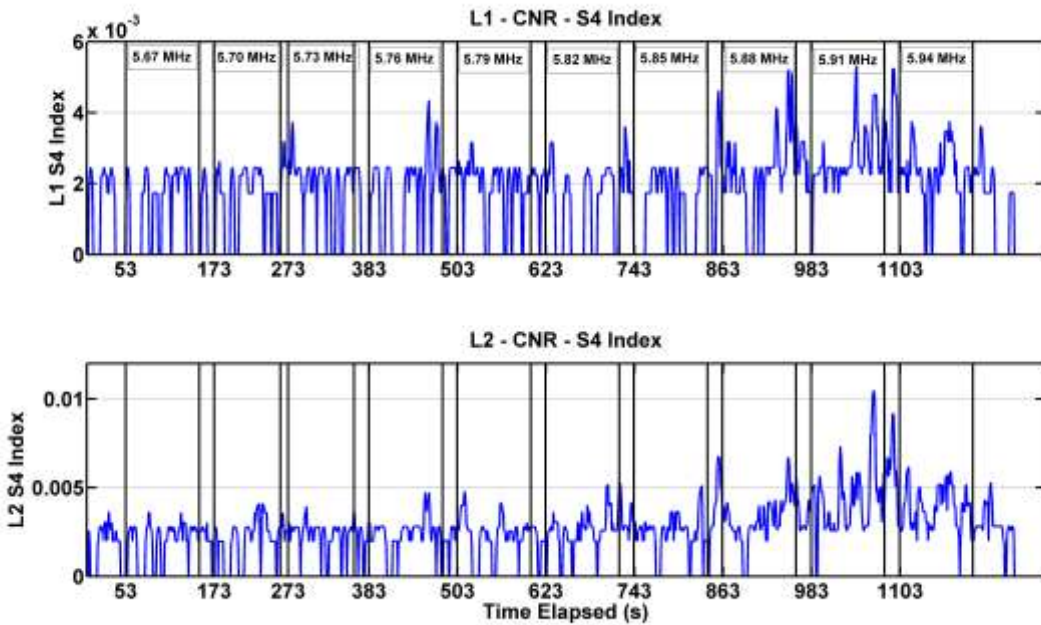
Figure 3b:

Figure 3: Scintillation index S_4 of the L1 and L2 Carrier-Noise-Ratio (CNR) vs. time elapsed and heating frequency on a) June 6th and b) June 7th. Heater on-off times indicated by solid vertical lines.
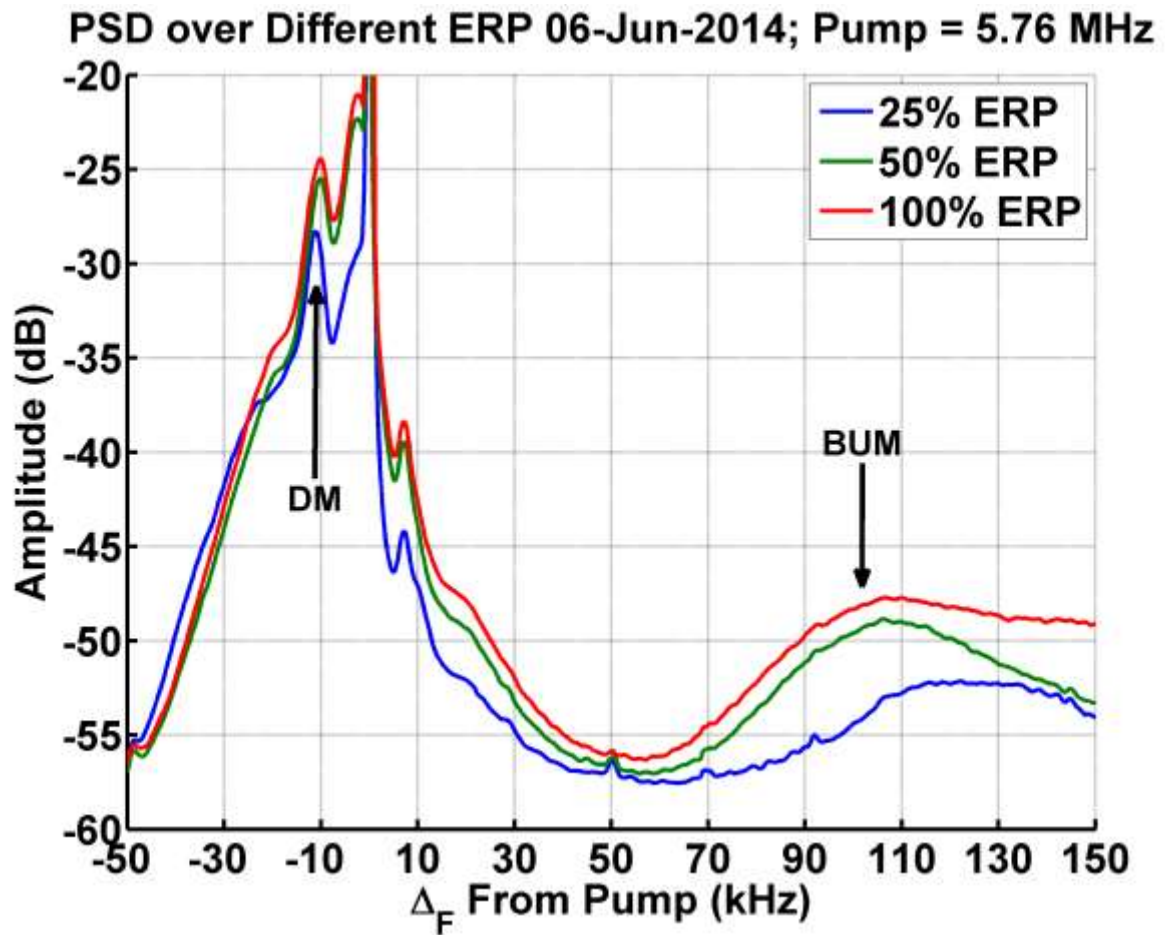
Figure 4: Power spectral densities (PSD) of broadband SEE from 06-Jun-2014 computed for the selected frequency 5.76 MHz. The traces are averaged over a 10s portion of the heating period with constant effective radiated power (ERP). The heating frequency is shown by the highest peak in the center at $\Delta_F=0$, the down shifted maximum (DM) is on the left side of the heating frequency while the broad upshifted maximum (BUM) is on the right side of the plots, both are indicated by arrows. The blue trace corresponds to the power 2.5 kW, green to 5.0 kW and red to 10 kW per transmitter (the power level 25, 50, and 100% respectively).
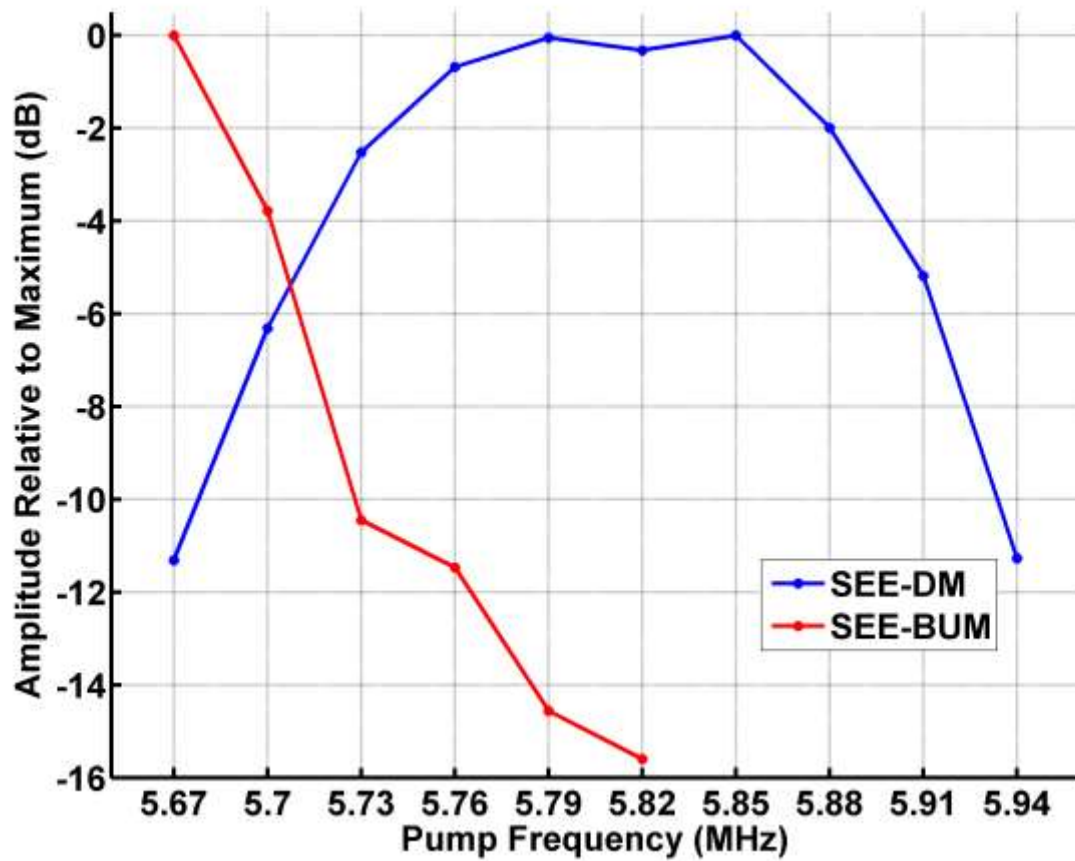
Figure 5: The red and blue traces show the amplitude of the BUM and DM respectively, both normalized by their peak values, as a function of the pump frequency.
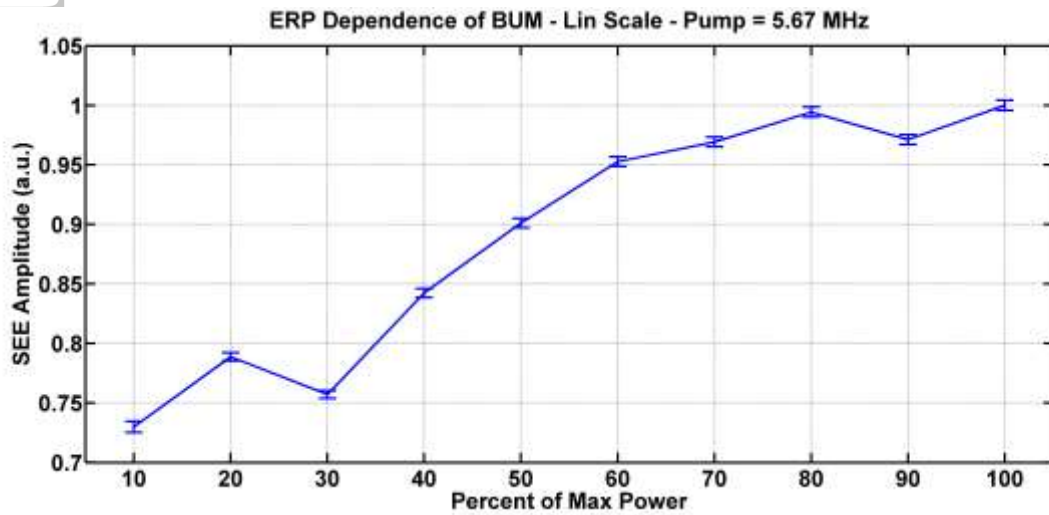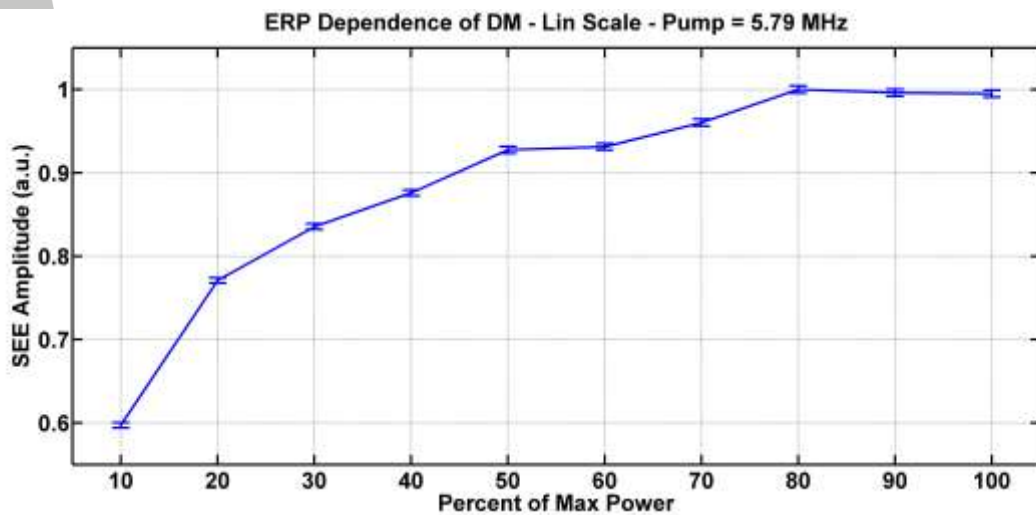
Figure 6a:

Figure 6b:

Figure 6: BUM (a) and DM (b) amplitude dependence on power. We chose the strongest values of the BUM and DM amplitude which are reached at 5.67 and 5.79 MHz respectively.
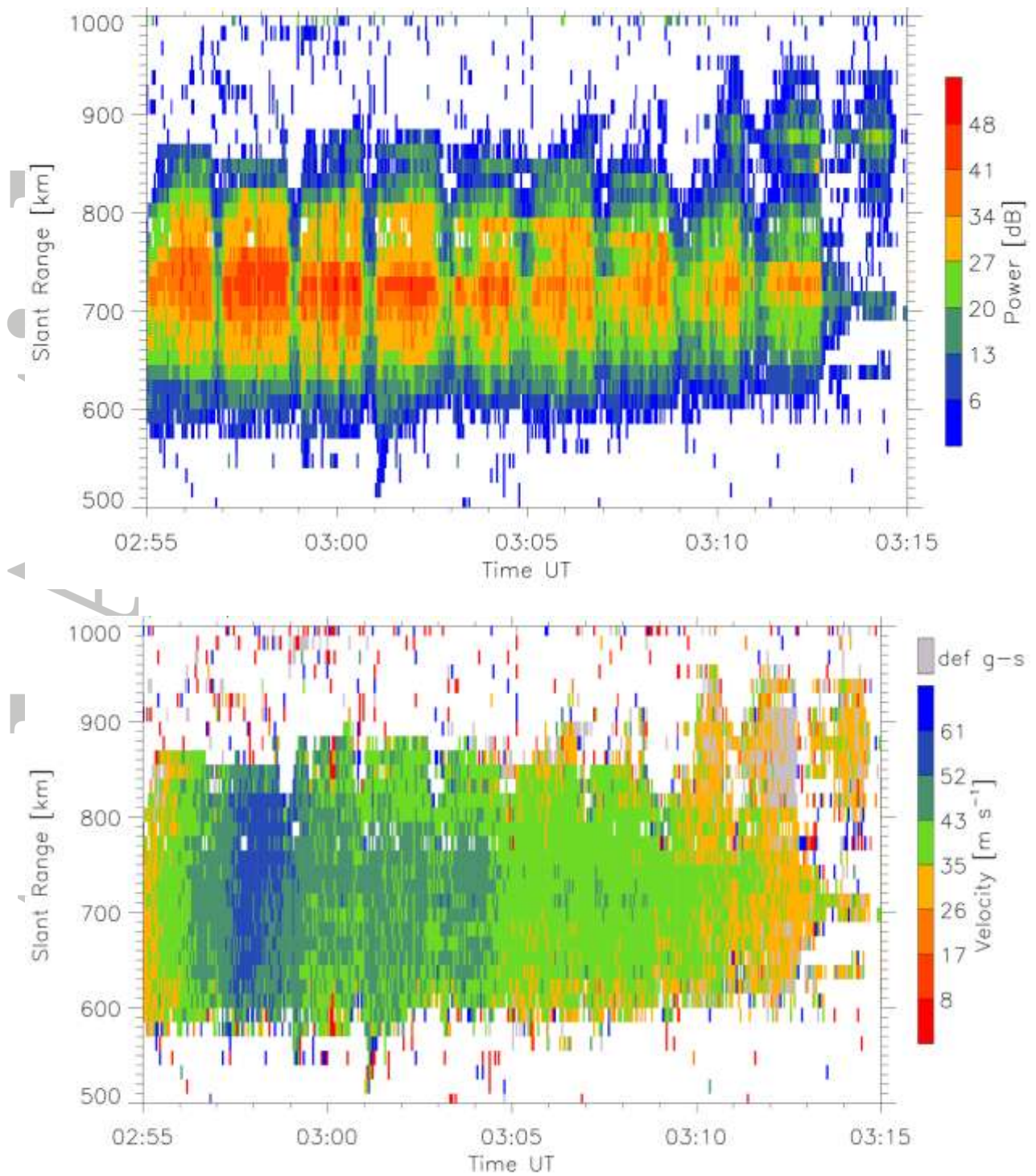
Figure 7: a) SuperDARN SNR from Kodiak Beam 09, b) velocity of plasma irregularities, all detected on June 6th. Slant range is approximate distance from Kodiak to an ionospheric reflector.
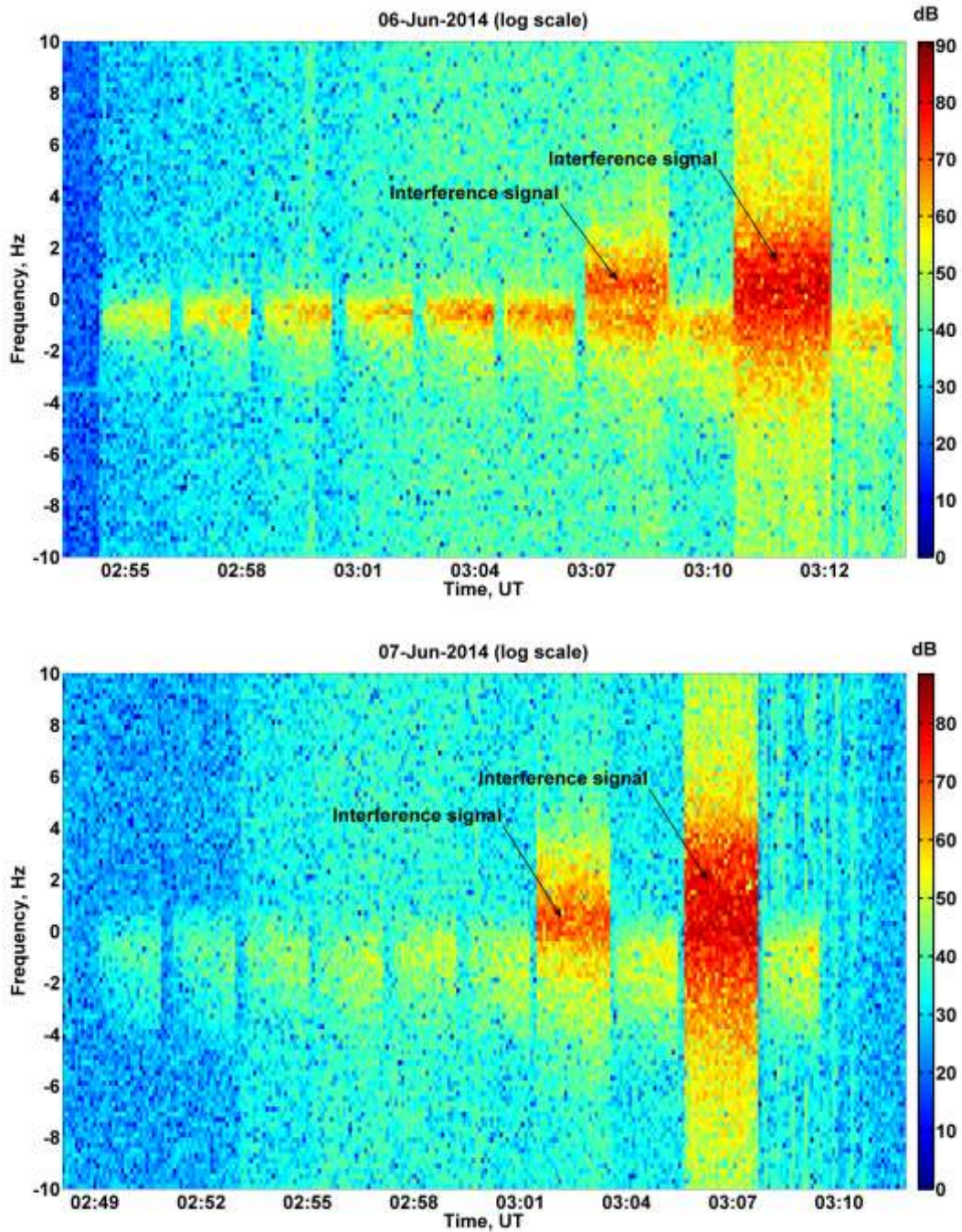
Figure 8: Spectrogram of received HF signal at UAS a) June 6th, b) June 7th. The 8th (f_h = 5850 kHz) and 9th (f_h = 5910 kHz) heating cycles, indicated by black arrows at the spectrograms, were contaminated by interference signals and therefore were not processed.
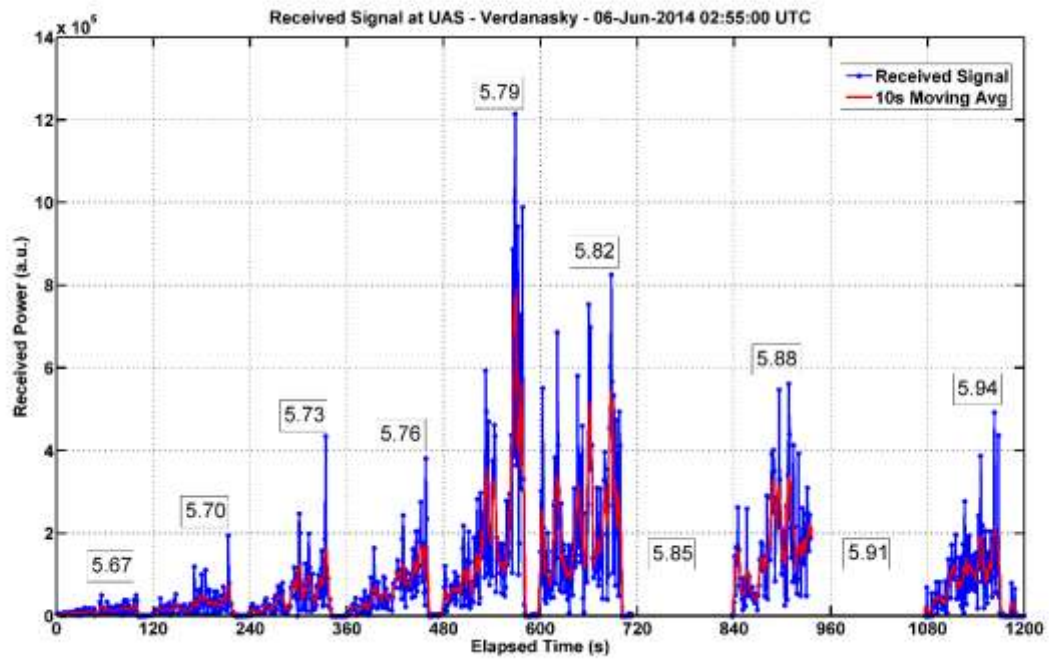
Figure 9: Time series of Received Power at UAS on June 6th with HF heating frequencies indicated. The intensity of the HAARP signals at the different heating frequencies is shown by the blue lines with the linear interpolation shown by the red lines.
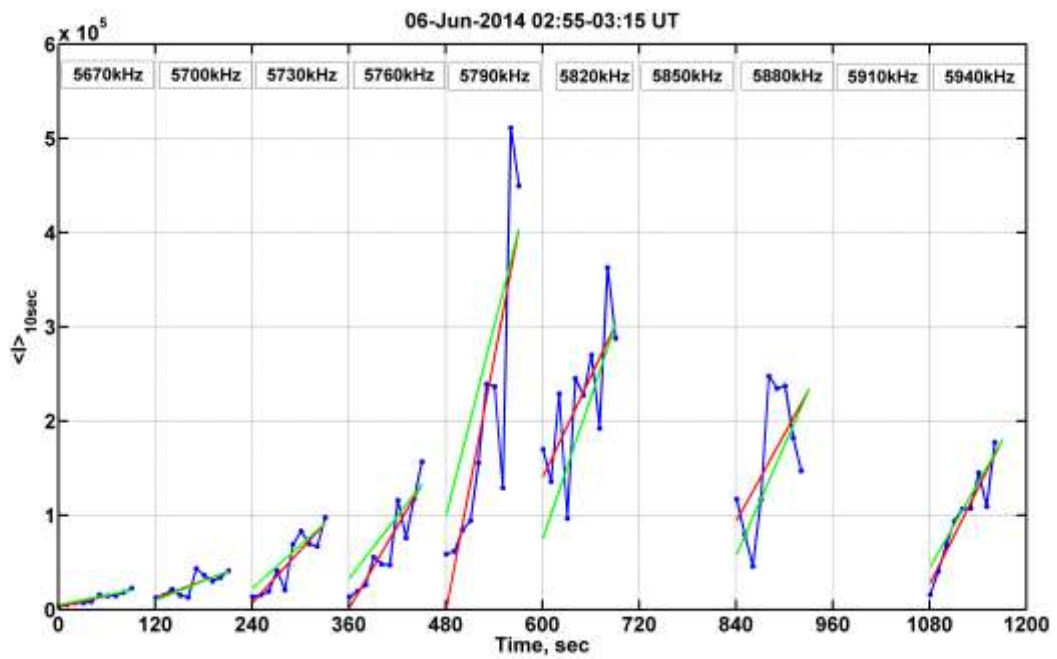
Figure 10: Scaling of Received Power at UAS with ERP. The intensity of the received signals at the different heating frequencies is shown by the blue lines. The green lines correspond to 4 times increase of the heating power, with the linear interpolation shown by the red lines.
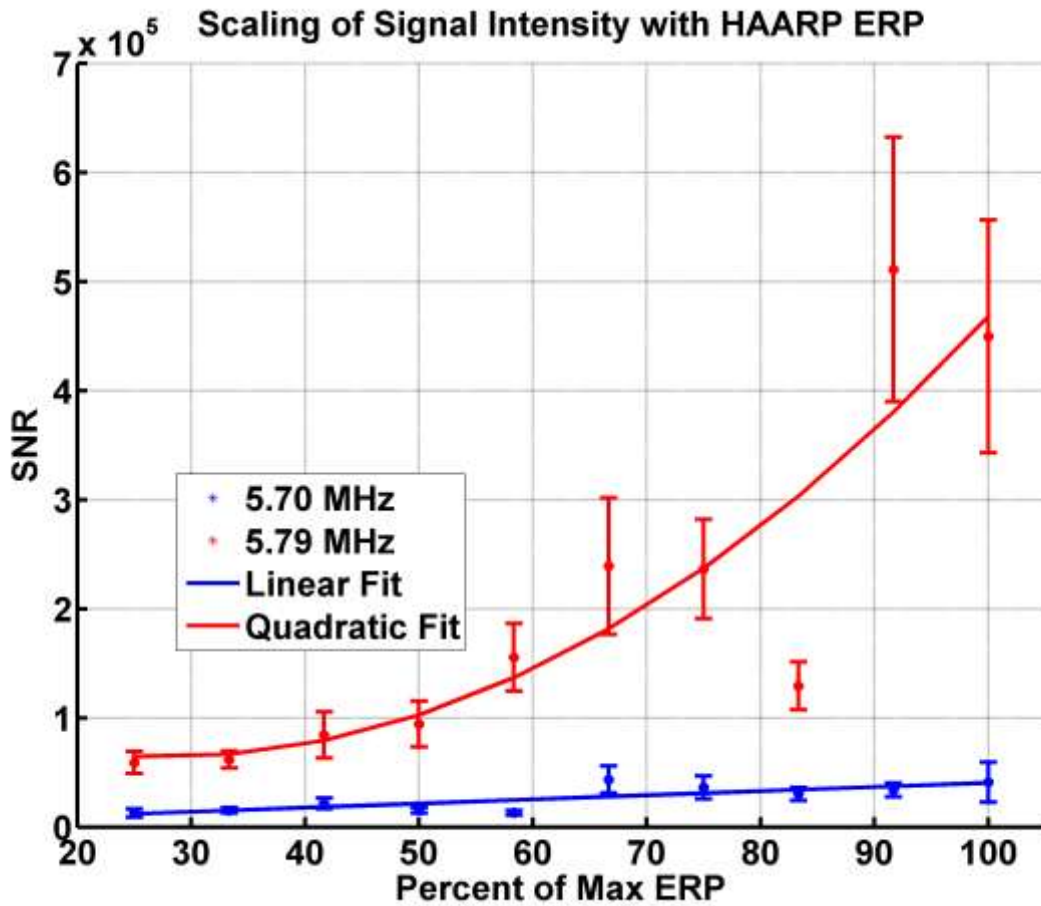
Figure 11: Scaling of the Signal-to-noise-ratio at UAS with ERP for two different pump frequencies. In blue, 5.70 MHz which is linear in HAARP's ERP, and in red, 5.79 MHz, which is non-linear in HAARP's ERP. Error bars are the standard deviation of the mean of SNR measured at UAS during heating at the given ERP and frequency.
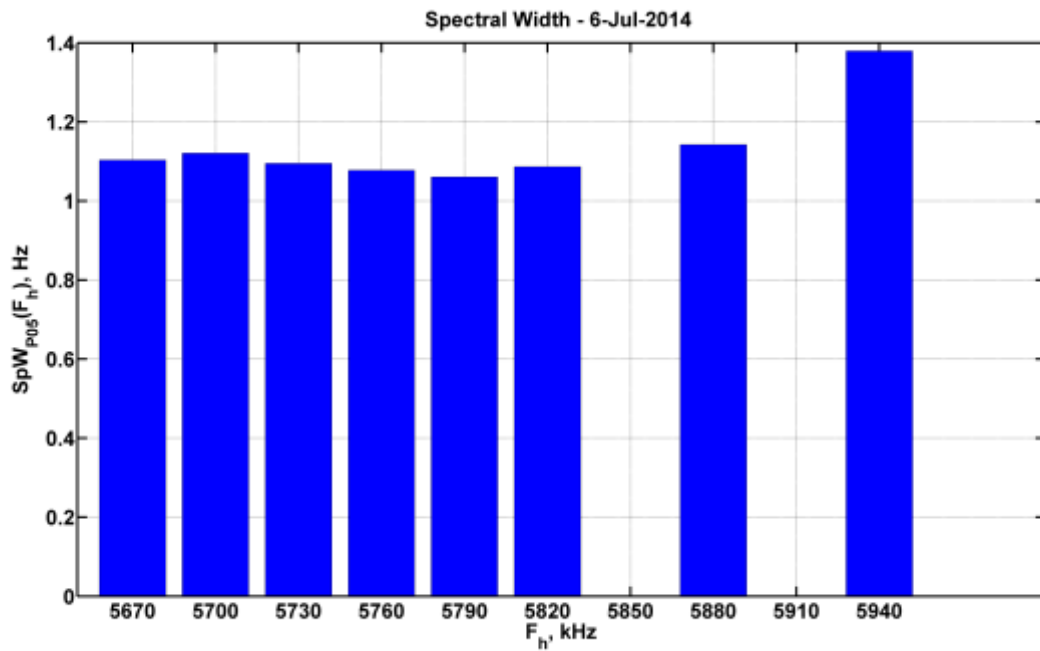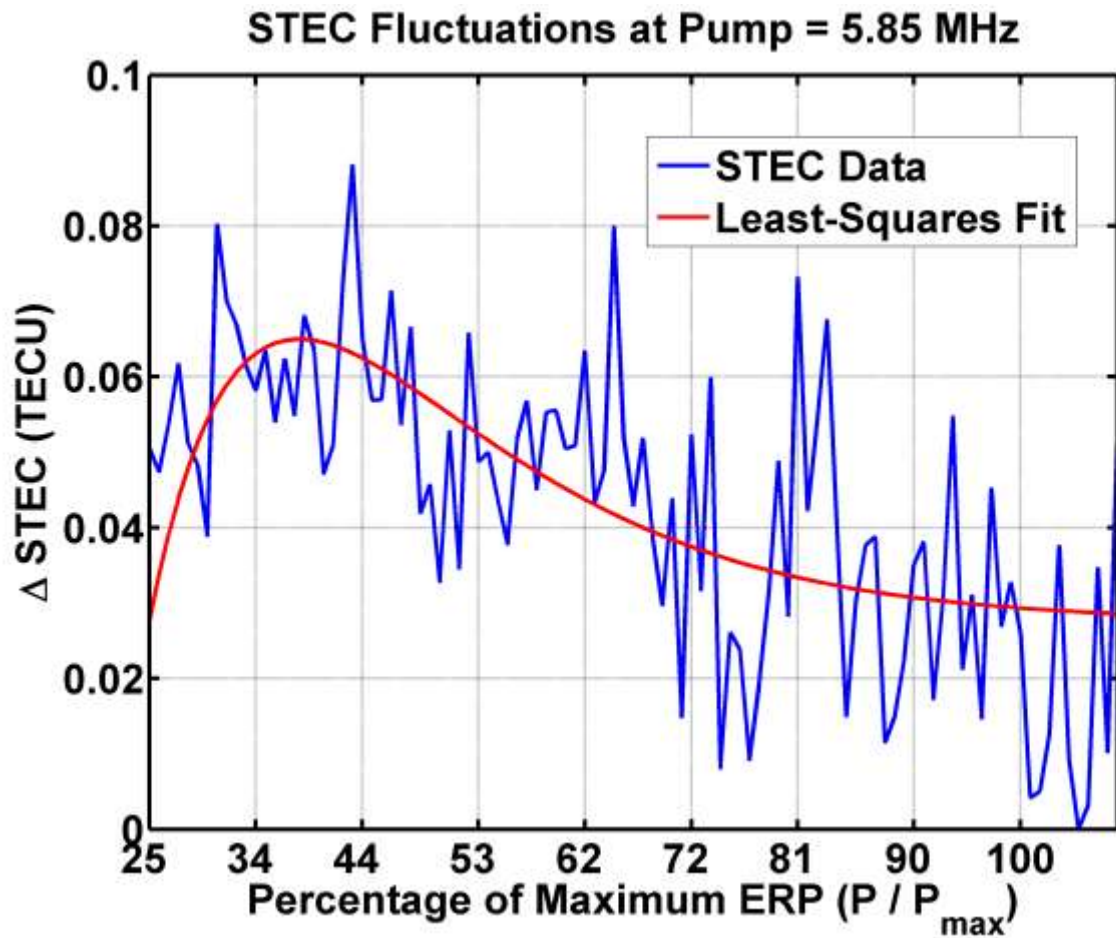
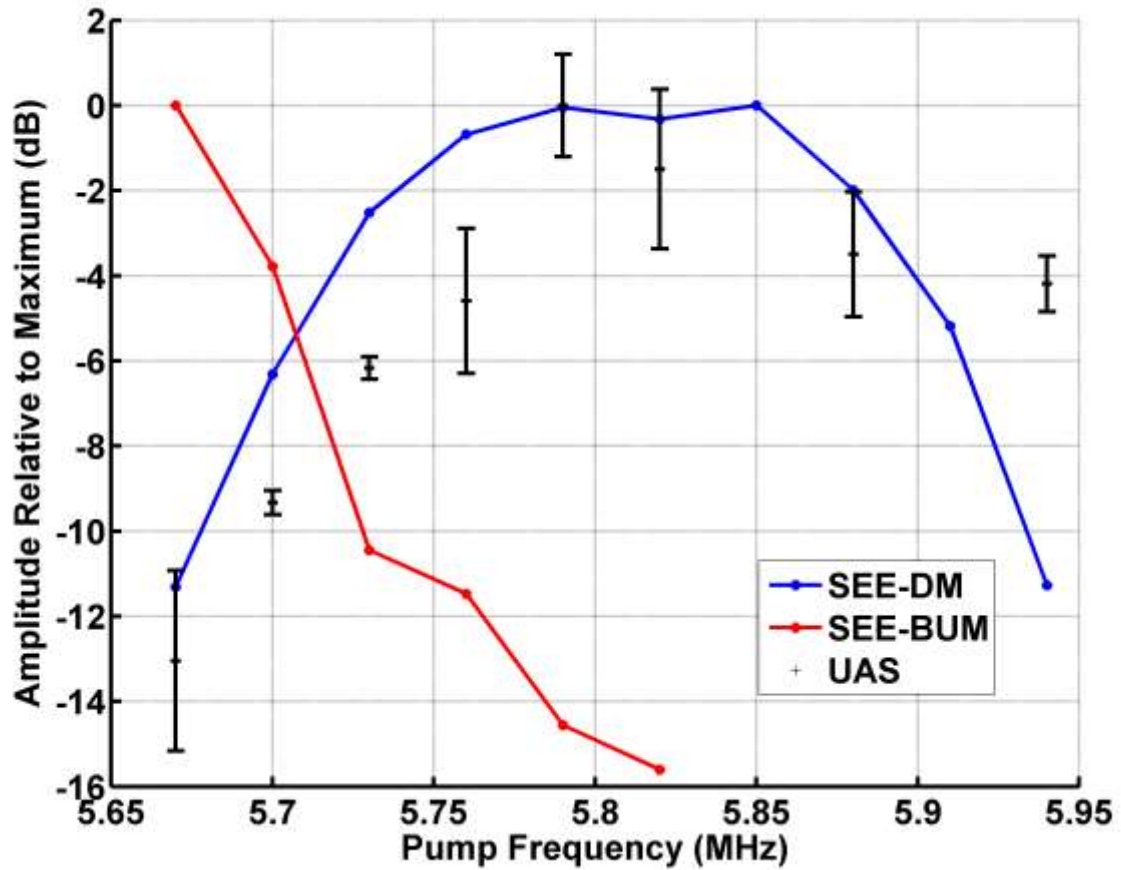**Figure 12**: Spectral width of received signal at half-max power at UAS vs. heating frequency measured on June 6th.
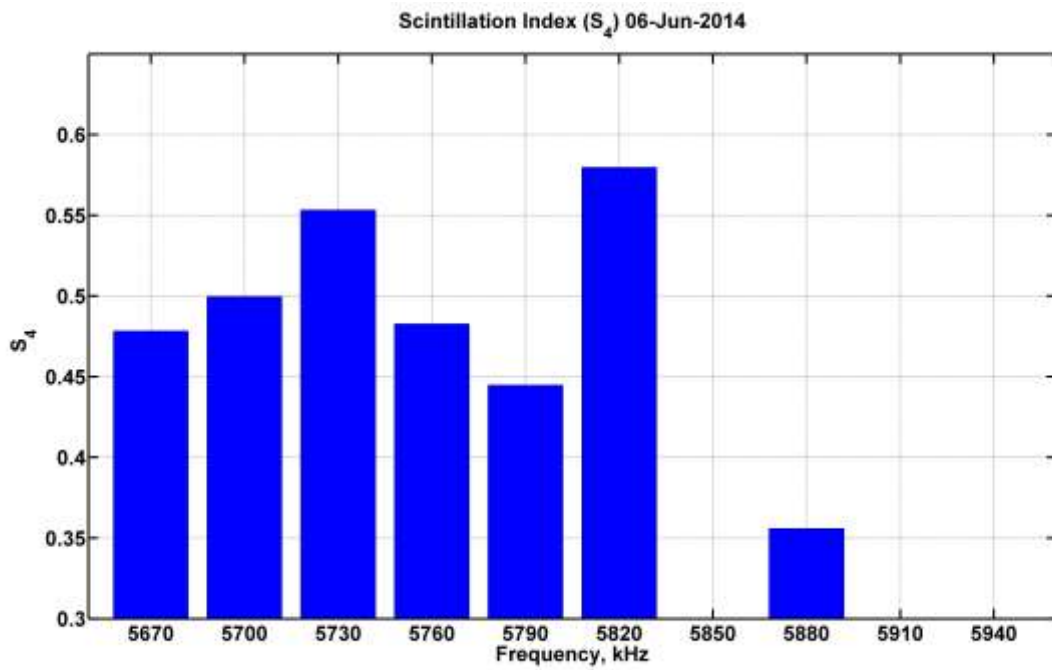
Figure 13: Scintillation Index (S$_4$) of Received Power at UAS as a function of heating frequency measured on June 6th.

Figure 14: STEC fluctuations as a function of ERP with least-squares fit to $xe^{-\alpha x}$, where x is the ratio of the HAARP ERP to its maximum ERP.

Figure 15: Amplitudes of DM (blue trace), BUM (red trace), and received power at UAS (black,with bars) relative to maximum values, as a function of the pump frequency. All data points are time averages over measurements taken at maximum ERP at the listed frequency are are normalized independently so that the maximum of each trace maps to 0 dB. All measurements taken on June 6th. Error bars of the black trace are the standard deviation of the mean of SNR measured at UAS during maximum ERP.

Table 1. Summary of Experiment beam angles. The listed initial zenith and azimuth angles are updated every five minutes to track the path of PRN 25.

Date	Start Time	End Time	Ini Angle,	+5 min	+10 min	+15 min
06/06/14	02:55	03:15	15.8, 220.9	16.1, 212.2	16.8, 204.1	17.4, 199.6
06/07/14	02:50	03:10	15.8, 222.4	16.0, 213.6	16.7, 205.4	17.2, 200.8